Delft University of Technology

Influence of Soret effect on flame structure and NO$_x$ emissions in highly strained lean premixed counterflow hydrogen flames

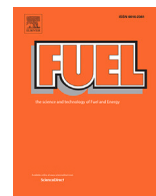Acquaviva, Maria Rosaria; Porcarelli, Alessandro; Langella, Ivan

Important note
To cite this publication, please use the final published version (if applicable).
Please check the document version above.

Full length article

Influence of Soret effect on flame structure and NO_x emissions in highly strained lean premixed counterflow hydrogen flames

Maria Rosaria Acquaviva* , Alessandro Porcarelli , Ivan Langella

Faculty of Aerospace Engineering, TU Delft, Kluyverweg 1, Delft, 2629 HS, Netherlands

HIGHLIGHTS

- The point of sign inversion of the Markstein length associated with strain shifts to richer equivalence ratios when Soret effect is taken into account.
- The prediction of NO emissions is strongly influenced by Soret effect as it impacts the local accuracy of the radicals concentration, especially under very lean conditions.
- Preferential diffusion (as opposed to the Lewis number effect) is the main driver of the Soret effect on the NO production trends with strain rate.
- Soret effect has a significant impact on the NO production rate, even at high pressure.

GRAPHICAL ABSTRACT
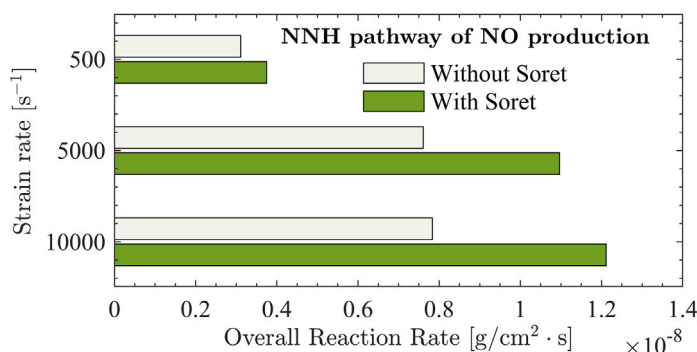
ABSTRACT

The influence of Soret effect on the prediction of flame characteristics and NO_x emissions in lean premixed hydrogen flames is studied in a reactant-to-product counterflow configuration under high strain conditions. By means of one-dimensional detailed chemistry simulations, the impact of Soret effect on the response of the flame to strain is first analyzed. The results show that leaner mixtures exhibit a stronger sensitivity to strain, and modeling thermal diffusion further intensifies this behaviour by affecting the prediction of temperature, peak of radicals, and consumption speed. Moreover, the Markstein length prediction is found to be affected by the thermal diffusion, with the main effect being to shift the point of sign inversion to a richer equivalence ratio as compared to the case where Soret effect is not considered. Isolating the hydrogen preferential diffusion and Lewis number effect, it is found that the response to strain is mainly driven by the Lewis number effect. Nevertheless, preferential diffusion behaviour is still observed to play a significant role in the leaning of the mixture ahead of the flame when Soret effect is taken into account. In terms of NO_x emissions, including thermal diffusion in the modeling causes an increase in both the peaks of NO mass fraction and its formation rate, especially under ultra-lean conditions where NO formation is primarily through the NNH pathway. The profiles of NO production rate with strain are also influenced, with prediction discrepancies ranging from 10 % in moderately lean conditions to 30 % in ultra-lean conditions. These effects are observed to be mainly associated to the preferential diffusion (as opposed to non-unity Lewis number effect) and its coupling with strain. Effect of pressure is also investigated, showing that the thermal diffusion can significantly alter the rate of production of NO even at high pressure conditions.

* Corresponding author.
  Email addresses: M.R.Acquaviva@tudelft.nl (M.R. Acquaviva), A.Porcarelli@tudelft.nl (A. Porcarelli), I.Langella@tudelft.nl (I. Langella).

1. Introduction

The global warming crisis and the ever increasing energy consumption imply there is an urgent need for research into renewable and low-carbon energy sources that can drastically reduce our dependence on fossil fuels [1]. In this scenario, hydrogen has the potential to be the candidate clean fuel to meet the net-zero CO_2 emission target [2]. Indeed, hydrogen combustion is expected to play a pivotal role in sectors such as aviation, where direct electrification from renewable resources is challenging. Owing to its very high low heating value (LHV), which is 2.5 times that of aviation kerosene, hydrogen is suitable for the aviation industry, especially for medium-haul flights niche [3]. On the other hand, hydrogen combustion still produces significant levels of toxic nitric oxides (NO_x) that can be mitigated by burning hydrogen in lean premixed conditions. Lean combustion, however, introduces a range of challenges, particularly due to hydrogen's high molecular diffusivity, which gives rise to non-unity Lewis and preferential diffusion effects. These effects can significantly influence both the flame speed and heat release rate. The non-unity Lewis number effect, also referred as Lewis number effect or diffusional-thermal effect [4] or differential diffusion [5], arises from the disparity in the molecular transport properties of hydrogen and thermal energy. Preferential diffusion, on the other hand, results from hydrogen's higher molecular diffusivity with respect to other species. In curved flame fronts, the non-unity Lewis number effect leads to the development of thermodiffusive instabilities [6], which are further promoted by preferential diffusion. For flat flame fronts, the non-unity Lewis number effect shapes the structure of the preheat zone, while preferential diffusion leads to local variations of the equivalence ratio [7–9]. Within this framework, the diffusive transport of hydrogen in lean flames is recently drawing much attention both for modeling purposes and for fundamental understanding of hydrogen combustion. Driven by temperature gradients, the Soret effect, also referred in the literature as thermodiffusion or thermal diffusion [10] (these nomenclature will be used interchangeably throughout this paper) is a secondary mass diffusion mechanism and it has often been neglected in flame simulations. Nevertheless, it can be relevant for species that are either extremely heavy or extremely light and in the presence of steep temperature gradients. Thus, it becomes crucial to understand its possible effects in the context of hydrogen/air flames, where both light and highly diffusive species (H_2, H) are present together with sharp temperature gradients associated with the strong heat release. Previous works [11] have shown that for lean strained hydrogen/air premixed flames, the Soret effect enhances the non-unity Lewis number effects as the thermal diffusion of the hydrogen molecule occurs in the same direction as the molecular diffusion. In addition, it further promotes the preferential diffusion effects, as the increased preferential transport of hydrogen towards the reaction zone modifies the local stoichiometry and consequently the fuel reaction rate [12]. However, few studies exist on the relevance of modeling thermal diffusion in premixed hydrogen flame under highly strained conditions where, as recently highlighted in [13], hydrogen/air premixed flames exhibit a very peculiar behaviour especially regarding the emissions outcome. For non-premixed flames, Williams [14] showed that the extinction strain rate vary by 20 % when predicted by different transport models, suggesting that the choice of a specific transport model might affect the prediction of the flame response to strain. The implications of modeling Soret effect in stretched and unstretched stoichiometric hydrogen-enriched syngas flames were also investigated by Liang et al. [15]. At atmospheric conditions, they found that the impact of Soret effect on the propagation of positively-stretched spherical flames is both to reduce the stretched flame speed and the Markstein length. Also, by means of a theoretical one-step chemistry model, Garcia-Ybarra et al. [16] observed that unlike for hydrocarbons, the thermal diffusion affects the value of the Markstein number in hydrogen/air flames. Furthermore, it has been shown that accounting for Soret effect leads to predict a lower unstretched laminar flame speed in lean conditions [17], but that the

extinction limit in strained conditions is also delayed [11]. Recently, Acampora and Marra [18] have shown how Soret effect can also impact indirectly the energy loss in premixed hydrogen/air unstrained flames. Furthermore, focus of recent investigation has been the role played by the Soret effect on the initiation and growth of thermodiffusive instabilities. For instance, Direct Numerical Simulations (DNS) of lean premixed hydrogen/air flames have demonstrated that the Soret effect enhances intrinsic flame instabilities [19]. Similarly, DNS of premixed ammonia/hydrogen flames has revealed that the Soret effect reduces the critical wavelength and increases the growth of instabilities, thereby promoting thermodiffusive instabilities [20].

So far, all of these studies have emphasized the significance of modeling thermal diffusion to accurately predict the flame dynamics, the temperature profiles, along with their response to strain. It is still unclear, however, whether considering the thermal diffusion might quantitatively affect the prediction of NO_x emissions. Only a few works have investigated the impact of thermal diffusion on NO_x production, such as recent DNS studies on NO_x emissions in thermodiffusively unstable lean hydrogen/ammonia [21] and pure hydrogen flames [22]. DNS of pure hydrogen flames, with the inclusion of the Soret effect, has shown that NO_x formation is mainly driven by the NNH pathway in positively curved regions due to the accumulation of H radicals, while NO production through the N_2O pathway prevails in negatively curved regions. Nevertheless, to the best of the author's knowledge, there are no studies explicitly analyzing the implications of modeling thermal diffusion on the prediction of NO_x emissions in lean premixed hydrogen flames subjected solely to high strain, without the influence of curvature effects. This condition has recently been shown to be relevant for the NO_x emissions trend with strain rate [13]. In the present work, the counterflow lean premixed hydrogen flame is numerically investigated to comprehensively assess the thermal diffusion effect on the NO_x emissions prediction in lean hydrogen/air premixed flames under high strain conditions. Results indicate that the Soret effect enhances the coupling between strain and the Lewis number effect, making the flame more resistant to strain itself, and this enhancement is stronger at ultra-lean conditions. Moreover, Soret effects is observed to shift the point of inversion of the Markstein length towards higher equivalence ratios and alter the trend of NO production rate with strain. It is found that the response of the flame to strain is mostly driven by the Lewis number effect. Nevertheless, the preferential diffusion behaviour (faster diffusion of hydrogen as compared to other species) influences quantitative predictions of NO_x concentration and production rate, when Soret effect is taken into account. Eventually, the Soret effect is still observed to play a significant role at high pressure conditions.

This work is organized as follows: Section 2 outlines the methodology employed in this study, including the governing equations reported in Section 2.1. Section 2.2 details the features of the computational setup. The primary effect of thermal diffusion on the response of the flame to strain is discussed in Section 3.1 with details on the behaviour of the local equivalence ratio in Subsec 3.1.1 and consumption speed and Markstein length in Section 3.1.2. Section 3.1.3 presents results obtained by analyzing the relative importance between Lewis number effect and preferential diffusion. The effect of thermal diffusion on NO_x emissions is presented in Section 3.2, by analyzing its influence on the NO mass fraction profiles (Section 3.2.1), global production rate and radical distribution (Section 3.2.2), effect of preferential diffusion and the Lewis number effect modeling (Section 3.2.3) and effect of pressure (Section 3.2.4). The main conclusions are summarized in Section 4.

2. Methodology

2.1. Governing equations

Similar to previous studies [23], planar counterflow premixed flames in a reactants-to-products configuration are employed in this work. As outlined in [13], such configuration allows for the achievement of

complete combustion even at high strain rates. Premixed hydrogen/air flame computations are performed with the code CHEM1D [24], widely employed for one-dimensional flame simulations [25] where the set of conservation equations solved reads:

$$\frac{\partial \rho}{\partial t} + \frac{\partial (\rho u_x)}{\partial x} = -\rho K, \tag{1a}$$

$$\frac{\partial (\rho Y_i)}{\partial t} + \frac{\partial (\rho u_x Y_i)}{\partial x} = -\frac{\partial (\rho V_{x,i} Y_i)}{\partial x} + W_i \dot{\omega}_i - \rho K Y_i, \tag{1b}$$

$$\frac{\partial (\rho h)}{\partial t} + \frac{\partial (\rho u_x h)}{\partial x} = -\frac{\partial q}{\partial x} - \rho K h, \tag{1c}$$

$$\frac{\partial (\rho K)}{\partial t} + (\rho u_x)\frac{\partial K}{\partial x} = \frac{\partial}{\partial x}\left(\mu \frac{\partial K}{\partial x}\right) + \rho_p a^2 - \rho K. \tag{1d}$$

In Eq. (1) ρ is the density of the mixture, u_x is the velocity along the flamelet longitudinal coordinate x, Y_i denotes the mass fraction of the ith and W_i is the molar mass of the species. The species rate of production is denoted as $\dot{\omega}_i$ while ρ_p is the density of the products mixture. The enthalpy is indicated with h, and q represents the total heat flux. The applied strain rate a is defined as:

$$a = -\left(\frac{du_x}{dx}\right)_p, \tag{2}$$

while in K is the local strain rate defined as:

$$K(x) = \frac{\partial u_y}{\partial y}. \tag{3}$$

The relationship between a and K is that $K_{x\to\infty} = a$. The diffusion velocity $V_{x,i}$ of the ith species is modeled using Curtiss–Hirschfelder approximation [26] and it is given by three contributions:

$$V_{x,i} = V_{Y_{x,i}} + V_{T_{x,i}} + V_{C_{x,i}}. \tag{4}$$

$V_{Y_{x,i}}$ is the molecular diffusion velocity due to molar fractions gradients while $V_{T_{x,i}}$ is the thermal diffusion velocity and $V_{C_{x,i}}$ is the correction velocity, which is needed to satisfy mass conservation [27]. The most general form to model the molecular diffusion velocity is the well-known Stefan–Maxwell equation reported in Eqs. (5a) and (5b) where the species diffusion velocities are obtained by balancing the driving force of diffusion with the resistance induced by every other component in the mixture. In Eq. (5a) $D_{i,j}$ is the binary diffusion coefficient of species i and j, and d_i the driving force of diffusion on species i, whose expression is reported in Eq. (5b) which also includes the thermal diffusion, known as Soret effect.

$$\sum_{i=1}^{Ns}\frac{X_j X_i}{D_{i,j}}(V_{Y_{x,i}} - V_{Y_{j,i}}) = d_i, \tag{5a}$$

$$d_i = -\frac{dX_i}{dx} + \sum_{i=1}^{Ns}\left(\frac{X_i X_j}{\rho D_{i,j}}\right)\left(\frac{D_{T,j}}{Y_j} - \frac{D_{T,i}}{Y_i}\right)\frac{1}{T}\frac{dT}{dx}. \tag{5b}$$

Although accurate, such a model is computationally expensive and sometimes prohibitive, especially for turbulent flame simulations. Therefore, Mixture Averaged diffusion model is usually preferred as it offers rather good accuracy with substantially lower computational cost. In the Mixture Averaged diffusion model, the diffusion velocity $V_{Y_{x,i}}$ of the i species is modeled as in Eq. (6a) assuming that the diffusion of a given species relative to the others is equivalent to its diffusion relative to the entire mixture D_i^M.

$$V_{Y_{x,i}} = -\frac{D_i^M}{X_i}\frac{dX_i}{dx}, \qquad D_i^M = \frac{1 - Y_i}{\sum_{j\neq i}\frac{X_j}{D_{i,j}}}. \tag{6a}$$

Within this framework, the Soret effect is modeled using the model proposed by [28] and the correction velocity $V_{C_{x,i}}$ is included to ensure the condition $\sum_{i=1}^{Ns}(Y_i V_{x,i}) = 0$. This model has been compared in

preliminary analysis (not shown) to a multicomponent model for the counterflow configuration at a representative applied strain level of $a = 10000\,\mathrm{s}^{-1}$, showing negligible differences in terms of temperature and major species, and an error below 10 % on radicals.

2.2. Computational setup

Lean laminar hydrogen/air premixed flames in reactants-to-products configuration are simulated under atmospheric conditions. This configuration is preferred to stagnation point and twin flame configurations to avoid respectively flame-wall and flame-flame interactions and limit the possible presence of partially unburnt radicals as explained in [13]. A one-dimensional domain with a length of $L_x = 50$ cm is selected for the calculations. The solver utilizes an adaptive mesh algorithm to ensure adequate mesh refinement in the reaction zone. Species mole fractions and temperature are imposed at the reactants and products boundaries. On the reactants side, a Dirichlet boundary condition is applied, setting the temperature of the reactants to $T_r = 300$ K. Mole fractions of species are imposed according to the assigned value of the equivalence ratio ϕ. On the product side, the adiabatic flame temperature obtained from a freely-propagating hydrogen flamelet solution at the same equivalence ratio is imposed. Mole fractions of species on the products side are determined assuming complete combustion. The reason complete combustion products are used rather than the equilibrium products is to prevent the presence of radicals and NO_x emissions at the boundary, and with that to avoid any bias in the analysis of NO_x behaviour. Various magnitudes of the applied strain rate a are explored together with a wide range of lean equivalence ratios ϕ to assess in many different conditions the effect of thermal diffusion modeling on the flame response and NO_x emission. To investigate the effect of thermal diffusion both on flame main characteristics and on NO_x emissions, all simulations are run with two diffusion models, namely Mixture Averaged (MA) and Mixture Averaged with Soret effect (MA + S). In addition, the results obtained through MA and MA + S models are further compared to the one using Multi-Component (MC) and Multi-Component with Soret (MC + S) to highlight also the accuracy and the limits of the former models. The reaction kinetics is modeled with the UCSD mechanism [29] modified with the mechanism from Capurso et al. [30] for NO_x prediction. While the prediction accuracy for NO formation via the NNH route was not fully addressed in [30], such mechanism has been validated against premixed and diffusion flames, and it is shown to accurately predict the complex transport phenomena observed in lean hydrogen flames and the consequent NO formation dynamics [30].

3. Results and discussion

3.1. Importance of thermal diffusion on the flame's response to strain

3.1.1. Local equivalence ratio and species diffusion fluxes

The effect of thermal diffusion is first isolated by analyzing the distribution of the local equivalence ratio ϕ_ℓ as a function of the progress variable c (Fig. 1) for two different values of the equivalence ratio ϕ, namely $\phi = 0.4$ (top row in Fig. 1) and $\phi = 0.8$ (bottom row in Fig. 1). The progress variable c is based on the water mass fraction Y_{H_2O} and the local equivalence ratio is defined according to [31] as:

$$\phi_\ell = \frac{1}{\mu}\frac{Z_H}{Z_O}, \tag{7}$$

where $1/\mu$ is the stoichiometric ratio and Z_α is the elemental mass fraction of H and O elements [25].

Without the Soret effect (MA), both at $\phi = 0.4$ and 0.8 and over the three applied strain rates considered, the local equivalence ratio shows a local minimum (dip) in the preheating zone ($c < 0.5$), indicating a local leaning of the mixture, followed by an overshoot immediately after the reaction zone ($c > 0.8$), indicating a local enrichment. As shown in [7], the dip in the mixture fraction or equivalently in the local equivalence ratio is present also in unstretched flames due to preferential diffusion.
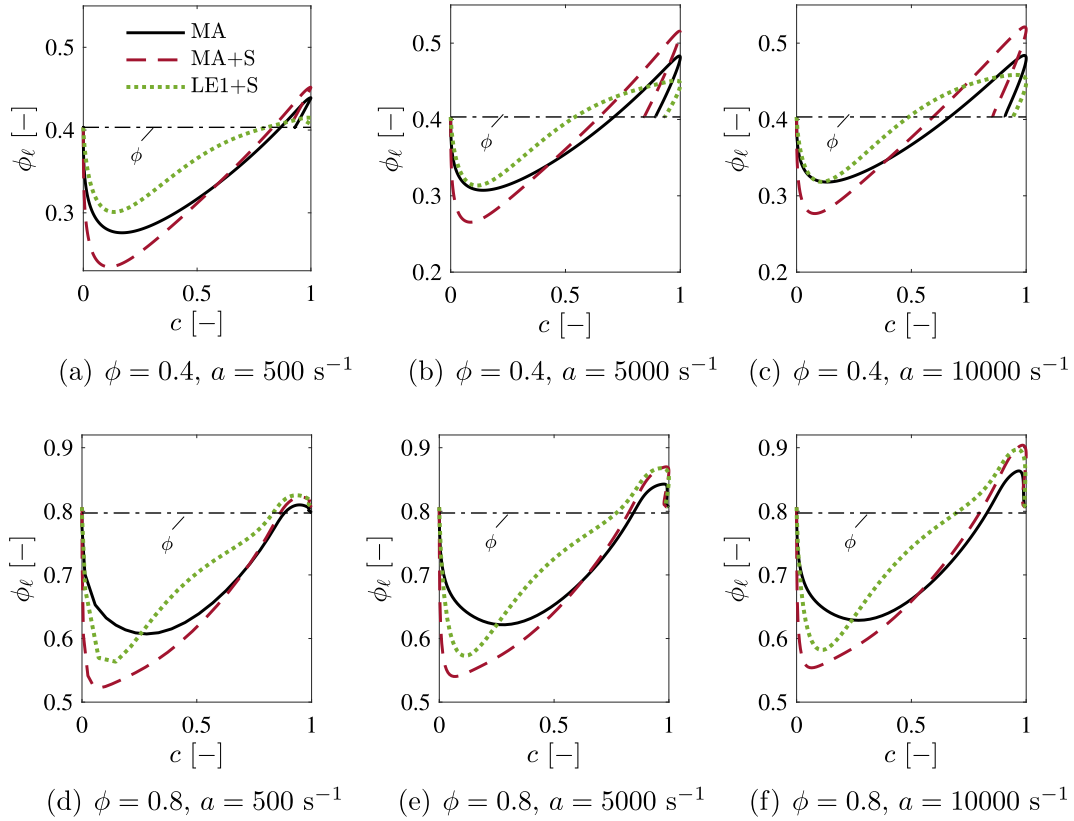
Fig. 1. Distribution of local equivalence ratio ϕ_ℓ as a function of the progress variable c for three values of the applied strain rate a. The acronyms in the legend refer to the Mixture Averaged (MA), Mixture Averaged with Soret effect (MA + S), and unity-Lewis number with Soret effect (LE1 + S) diffusion models. $\phi = 0.4$ (top) and $\phi = 0.8$ (bottom).

Conversely, the overshoot (values higher than the nominal value of ϕ) is present only when a stretched configuration is considered. This is consistent with the fact that for the lower strain rate considered, namely $500 \ \mathrm{s}^{-1}$ (Fig. 1a), the overshoot is rather negligible; instead, when the strain rate increases up to $a = 10000 \ \mathrm{s}^{-1}$ (Fig. 1c) the overshoot becomes more evident. Moreover, comparing the dip obtained across the different strain values (Fig. 1a–c), it can be seen that the local reduction of the equivalence ratio is more limited at increasing strain rate. As previously noted, these overshoots are linked to the strain rate applied to the flame. The higher overshoots observed with the MA + S model indicate a greater sensitivity of the flame to strain. Furthermore, comparing the MA and MA + S models with a unity Lewis number model including the Soret effect (LE1 + S) (green dotted curves in Fig. 1), highlights that thermal diffusion alone can cause significant local shifts in equivalence ratio values at any strain rate, confirming the necessity of incorporating the Soret effect in species diffusion modeling.

Furthermore, by comparing the results at $\phi = 0.4$ (Figs. 1a–c) with those at $\phi = 0.8$ (Figs. 1d–f), it is clear that the local equivalence ratio is less influenced by the applied strain rate at $\phi = 0.8$. In fact, the variation in the dip and overshoot values of ϕ_ℓ is more limited when increasing the applied equivalence ratio. This different sensitivity to strain for the two equivalence ratio values can be linked to the trend of flame thickness with strain rate, displayed in Fig. 2. In fact, the strain rate reduces the flame thickness, which ultimately triggers an increase in the species and temperature gradients. Given that at the richer equivalence ratio the flame thickness is less significantly affected, the sensitivity to strain appears to be weaker.

To explain the increased deviation in the local equivalence ratio from the nominal value when the Soret effect is taken into account, the spatial distributions of the thermal and molecular diffusion fluxes
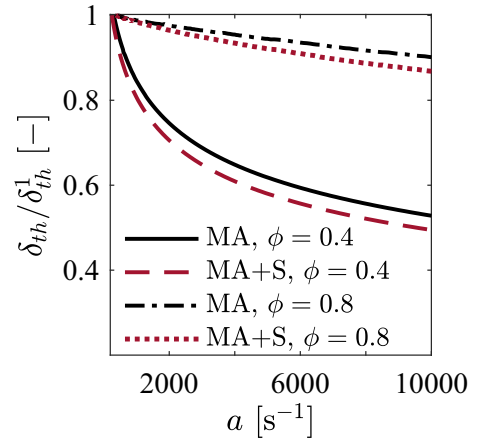

Fig. 2. Normalized flame thermal thickness δ_{th} as a function of the applied strain rate a. δ_{th}^1 is the flame thermal thickness at the lowest strain rate investigated $a = 500 \ \mathrm{s}^{-1}$. The acronyms in the legend refer to the Mixture Averaged (MA) and Mixture Averaged with Soret effect (MA + S) diffusion models.

of H_2 (Figs. 3a,c) and H (Figs. 3b,d) are presented. To compare the different curves obtained for different strain rate values, the x coordinate is shifted to align zero with the flame position x_0, and is made dimensionless with respect to the strained laminar flame thickness δ. By inspection of Fig. 3, it can be noted that both at $\phi = 0.4$ and $\phi = 0.8$ the combined effect of thermal and molecular diffusion fluxes results in a net diffusion flux of H_2 which increases the transport of hydrogen in the
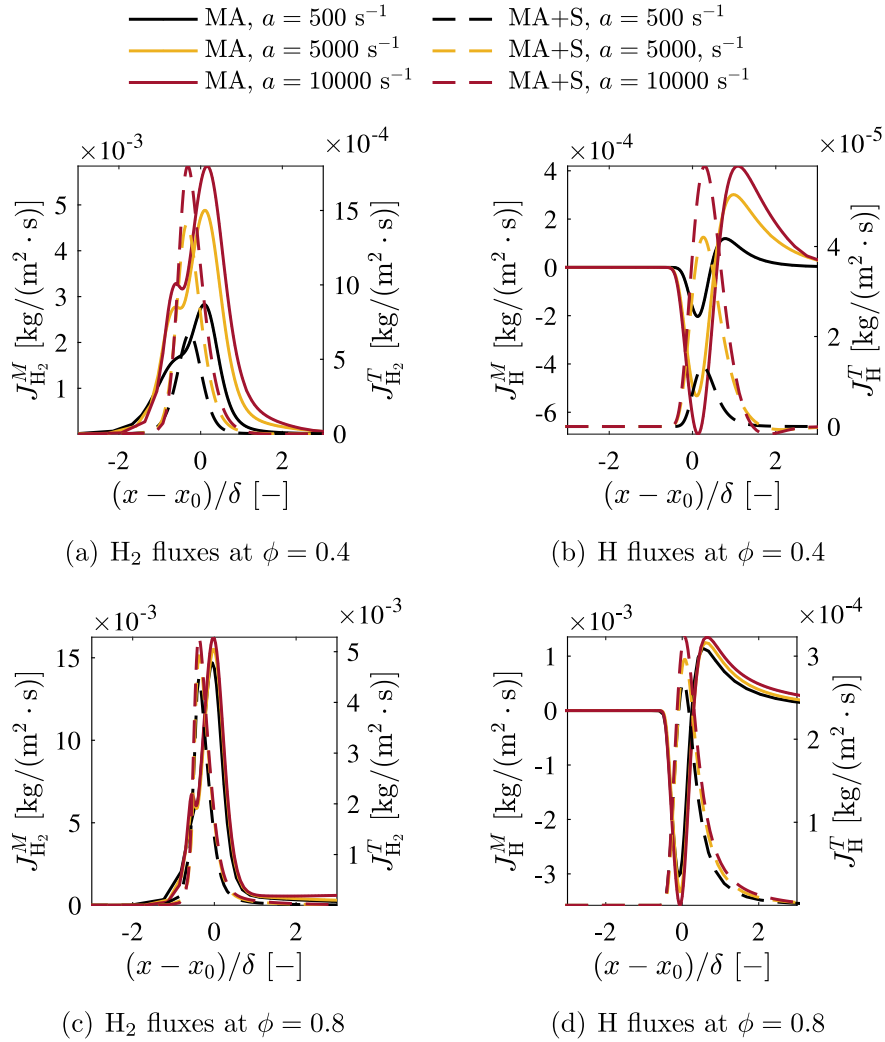
Fig. 3. Fickian (solid lines) and thermal diffusion (dashed lines) fluxes of H_2 (left column) and H (right column) at $\phi = 0.4$ (first row) and $\phi = 0.8$ (second row) for different applied strain rate, a, values.
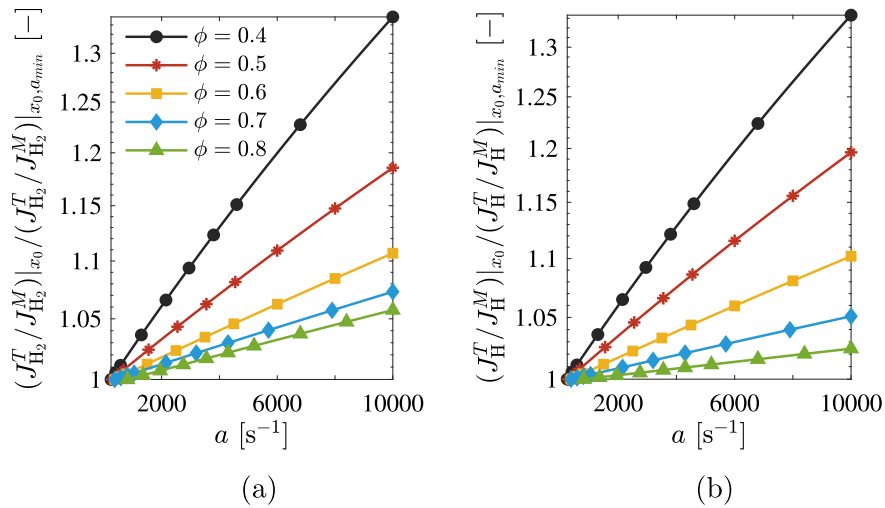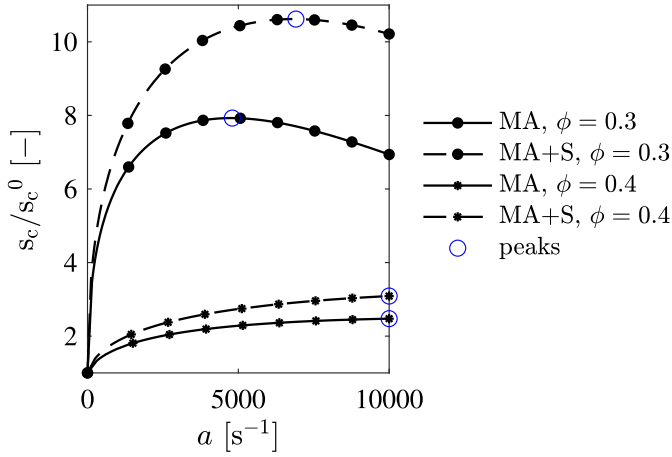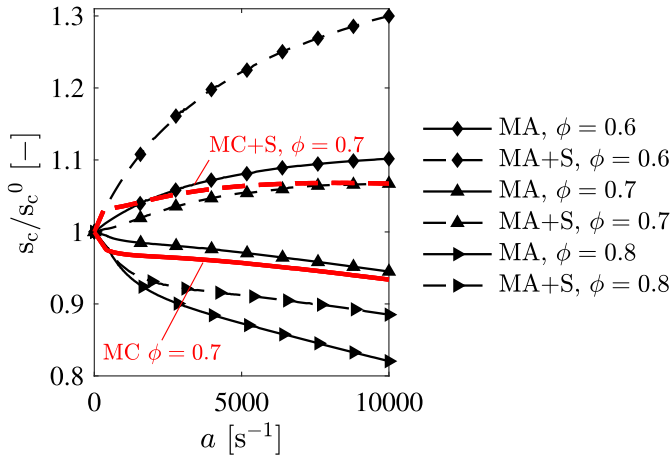

Fig. 4. Normalized ratios of thermal diffusion and molecular diffusion fluxes of H_2 (a) and H (b) with respect to the ratio at the minimum strain, $a_{min} = 500 \text{ s}^{-1}$, as a function of the applied strain rate a. The y-axis is in logarithmic scale.

(a)

(b)

Fig. 5. Normalized fuel consumption speed s_c with respect to the unstrained flame speed s_c^0 obtained through the Mixture Averaged (MA) and Mixture Averaged with Soret (MA+S) models as a function of the applied strain rate a. Results are shown for $\phi = 0.3, 0.4$ (a) and $\phi = 0.6, 0.7, 0.8$ (b).

Fig. 6. Strain rate Markstein length $\mathcal{L}_s$ as a function of the equivalence ratio ϕ obtained with Mixture Averaged (MA), Mixture Averaged with Soret effect (MA+S), Multi-Component (MC), and Multi-Component with Soret effect (MC+S) diffusion models. The red filled markers are the value of ϕ at which $\mathcal{L}_s = 0$. (For interpretation of the references to colour in this figure legend, the reader is referred to the web version of this article.)

Fig. 7. Contour plot of the absolute difference between the maximum temperature T_{max} obtained with Mixture Averaged (MA) and Mixture Averaged with Soret effect (MA+S) models.

reaction zone. This contributes to the previously discussed learning and enrichment effects. Conversely, as already observed in [32], the thermal diffusion flux of the H radical limits its diffusion in the reactant region, leading to an accumulation of H radical in the flame zone.

Further analysis is conducted on the relative importance between the molecular J_i^M and thermal J_i^T fluxes of species i = H$_2$, H. Specifically, in order to assess the relative importance between the two fluxes with increasing strain rate, the ratios of the thermal and molecular diffusion fluxes J_i^M/J_i^T are first calculated at the flame position x_0 and then normalized with respect to those obtained at the lowest strain rate investigated, namely $a = 500 \text{ s}^{-1}$ (Fig. 4). Although the thermal diffusion fluxes of H$_2$ and H are significantly lower than those due to Fickian diffusion (see Fig. 3), interesting trends emerge when looking at their normalized ratios with increasing strain rate and equivalence ratio. In particular, at $\phi = 0.4$ the ratio J_i^T/J_i^M for both H$_2$ and H is about 1.3 times higher as the strain rate increases from $a = 500 \text{ s}^{-1}$ to $a = 10000 \text{ s}^{-1}$, confirming that thermal diffusion has a greater influence at higher strain rates. On the other hand, the slopes of these curves decrease with increasing global equivalence ratio, confirming the weaker sensitivity of the flame to strain in these conditions. Yet, it should be remarked that in
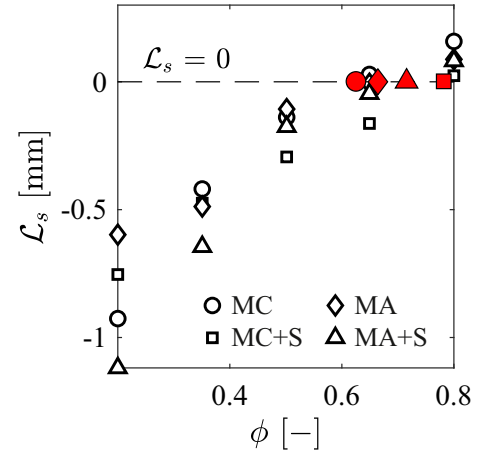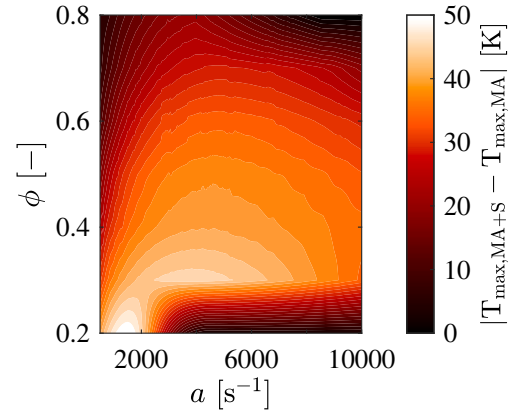
unstretched or low-strain conditions, thermal diffusion is stronger at the higher equivalence ratio, because both the shorter flame thickness (see Fig. 2) and the larger jump between reactants and product temperature trigger overall higher temperature gradients.

3.1.2. Consumption speed and markstein length

The response to strain of lean hydrogen premixed flames with Soret effect is further analyzed by studying the behaviour of the fuel consumption speed s_c. In fact, this quantity is sensitive to local stretch, especially in the presence of mixture non-equidiffusion effects [33]. The fuel consumption speed is computed as:

$$s_c = \frac{1}{\rho^1 Y_{H_2}^1} \int_{-L/2}^{L/2} \dot{\omega}_{H_2} \, dx, \tag{8}$$

with ρ^1 and $Y_{H_2}^1$ indicating the density and mass fraction of hydrogen at the reactants side.

Results are presented in Fig. 5a and b. To analyze the sensitivity of this global parameter to applied strain rates, the fuel consumption speed is normalized with respect to the fuel consumption speed of an
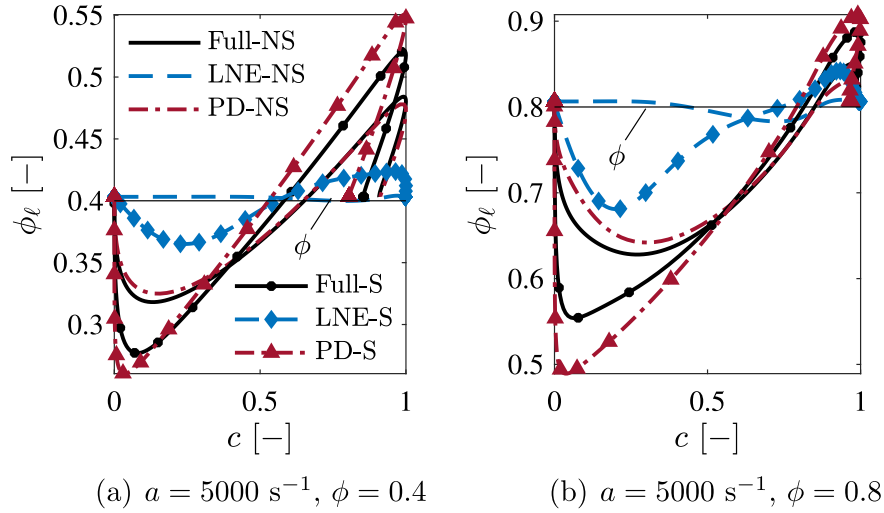
Fig. 8. Distribution of local equivalence ratio ϕ_ℓ as a function of progress variable c obtained with and without Soret effect, and by considering both preferential diffusion and Lewis number effects (Full-S and Full-NS cases), or their relative contributions in isolation (PD and LNE cases). The acronyms S and NS refer to inclusion or exclusion of Soret effect respectively.
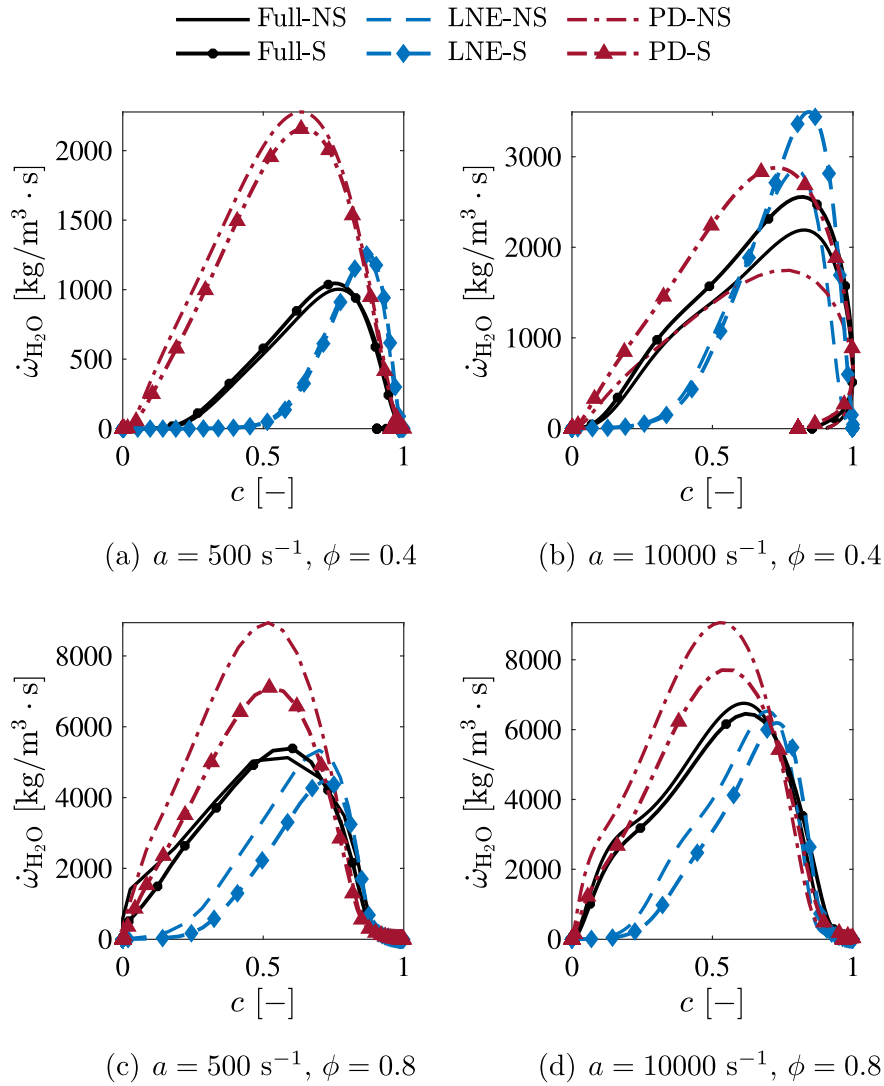
Fig. 9. Distribution of the water vapour reaction rate $\dot{\omega}_{H_2O}$ as a function of the progress variable c obtained with and without Soret effect, and by considering both preferential diffusion and Lewis number effects (Full-S and Full-NS cases), or their relative contributions in isolation (PD and LNE cases). The acronyms S and NS refer to inclusion or exclusion of Soret effect respectively.

Fig. 10. Comparison of the consumption speed values, normalized with respect to the unstrained value s_c^0 obtained with and without Soret effect, and by considering both preferential diffusion and Lewis number effects (Full-S and Full-NS cases), or their relative contributions in isolation (PD and LNE cases). The acronyms S and NS refer to inclusion or exclusion of Soret effect respectively.
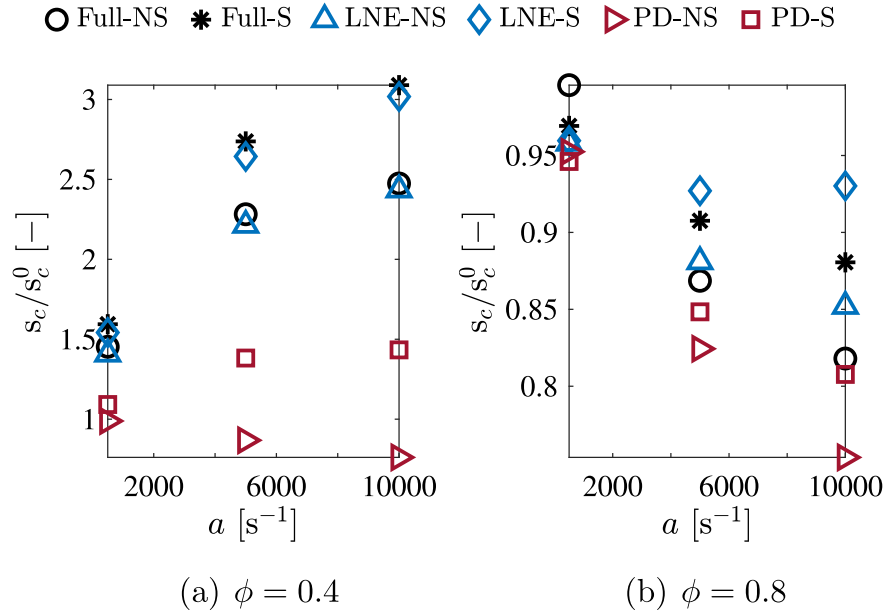
unstrained flame s_c^0 at the same equivalence ratio. At ultra-lean conditions (Fig. 5a) the fuel consumption speed increases with strain, as one would expect for lean hydrogen flames [33]. The thermal diffusion amplifies this effect, causing the peaks of consumption speed to shift towards higher strain rates (see blue circles in Fig. 5a). For instance, at $\phi = 0.3$ a peak in consumption speed is observed, whose location when Soret effect is included shifts from $a = 5000$ s^{-1} to $a = 7000$ s^{-1}, with a relative percentage deviation of up to 30 %. Note that this effect is evident primarily at very low equivalence ratios because the flame is close to strain-induced extinction at this condition. One can expect that a local maximum also exists for richer conditions, but this would occur at strain rate levels outside the range reported in Fig. 5a.

Under moderate lean conditions (Fig. 5b), the thermal diffusion still contributes to increase the fuel burning rate, despite the reduced sensitivity of the flame to strain. The fuel consumption speed enhancement due to the thermal diffusion is such that when s_c starts to decrease with strain (Fig. 5b lines at $\phi = 0.8$), the effect of thermal diffusion tends counteracts this reduction by mitigating the decrease in consumption speed with strain. The latter observation can be further clarified by looking at the behaviour of the Markstein length $\mathcal{L}_s$ with the applied strain rate, which is defined as:

$$\mathcal{L}_s = -\left.\frac{\partial s_c}{\partial a}\right|_{a=0}. \tag{9}$$

It is important to note that the given definition corresponds specifically to the strain rate Markstein length, as curvature effects are not analyzed in the present study [34]. The strain Markstein length obtained using the MA and MA + S models is presented as a function of the equivalence ratio in Fig. 6. To enhance confidence in the results obtained, a comparison is also made with data obtained using the MC and MC + S models. Focusing first on results obtained with MA and MA + S models in Fig. 6, it is seen that thermal diffusion tends to increase the absolute value of the strain Markstein length. As a consequence, the MA and MA + S models predict a different inversion point of the strain Markstein length, i.e. The value of ϕ at which $\mathcal{L}_s$ changes sign (see red markers in Fig. 6). Specifically, while the MA model predicts an inversion point at $\phi = 0.65$, the inclusion of the Soret effect shifts the inversion point to $\phi = 0.72$.

A similar trend is observed when using detailed multi-component models (MC and MC + S), confirming that regardless of the model employed, the inclusion of the Soret effect allows for a more accurate prediction of the flame's response to strain. In summary, the present analysis indicates that a flame initially weaker under unstretched conditions becomes globally more strengthened or less weakened by an increasing strain rate when thermal diffusion effects is accounted for. Additional evidence is provided in Fig. 7, which shows the difference of the maximum temperature between cases with and without the Soret effect across a wide range of ϕ and strain rates value. The maximum temperature becomes up to 50 K higher at lean conditions and at highest strain rate when the Soret effect is included, resulting from the overall increase in the burning rate. Therefore, modeling the Soret effect is crucial for accurately and quantitatively predicting the response of lean hydrogen flames to strain or stretch, especially in lean conditions. This is expected to be fundamental in predicting NO$_x$ emissions, which will be examined in the next section. Furthermore, the obtained results provide implications for flamelet-based methods applied to lean hydrogen/air-premixed flames. As also discussed in [35], stretch effects might be necessary at the thermochemistry level. Since the response to strain, as shown in the present work, changes when Soret effect is considered, this contribution has to be mimicked in flamelet models.

3.1.3. Relative contributions of non-unity Lewis number and preferential diffusion effect

The effect of thermal diffusion on the flame response to strain has been studied so far without explicitly accounting for its influence when isolating the Lewis number effect (the disparity between the deficient reactant and thermal energy transport) and hydrogen's preferential diffusion relative to other species. This distinction is addressed in this section. For this analysis, two equivalence ratio values, $\phi = 0.4$ and 0.8, along with three applied strain rates, $a = 500$, 5000, and 10000 s^{-1}, are selected. The effects of preferential and Lewis number effect are isolated following the approach described in [36]. Preferential diffusion is suppressed by setting the Lewis number of all species equal to that of hydrogen (the deficient reactant) (LNE case), while Lewis number effect is suppressed by scaling the Lewis numbers of all species to ensure a Lewis equal to one for the molecular hydrogen (PD case). Each case was then
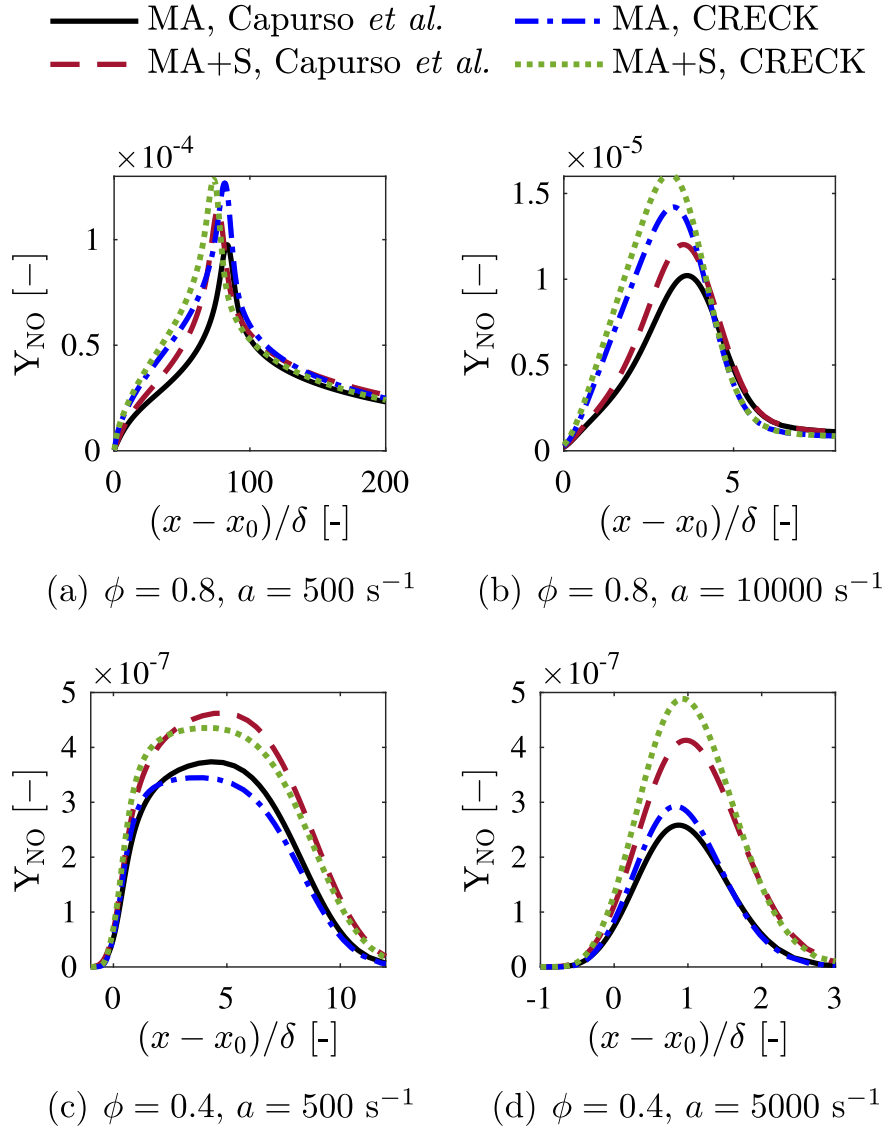
Fig. 11. Y_{NO} spatial profiles obtained using the detailed CRECK mechanism [37] and the mechanism proposed by Capurso et al. [30]. The acronyms in the legend refer to the Mixture Averaged (MA) and Mixture Averaged with Soret effect (MA + S) diffusion models.

analyzed both without (LNE-NS and PD-NS) and with the Soret effect (LNE-S and PD-S) and compared against the MA model, also considered with and without the Soret effect (Full-S and Full-NS). Consistently to what showed in Section 3.1, both at $\phi = 0.4$ and $\phi = 0.8$, the effect of Soret is mainly to increase the dips and the overshoots of local equivalence ratio for both PD and LNE cases (Figs. 8a,b). Moreover, by comparing the curves obtained for the PD and LNE cases to the Full-NS case, it becomes evident that the local variations in equivalence ratio are predominantly driven by preferential diffusion, as one would expect. However, when Soret effect is modeled, the Lewis number effect is also accountable for the leaning observed ahead the flame (see blue dashed curves with and without the diamond marker in Fig. 8a,b), although this remains limited to a secondary effect. By examining the distribution of the water vapour reaction rate in Fig. 9, one can notice that the peaks predicted by the Lewis number effect (LNE) cases align more closely with those of the Full cases. Moreover, the differences in reaction rate profiles between the Full-NS and Full-S cases are better captured when the Lewis number effect is modeled with the inclusion of Soret effects (see Full-NS and Full-S curves in Fig. 9). In addition, similar to the Full-S and Full-NS models, the LNE-S case shows a smaller deviation from the LNE-NS case at the lowest strain rate, $a = 500$ s^{-1}. Also, the LNE-S

model captures the increase at $\phi = 0.4$ and the slight decrease at $\phi = 0.8$ observed with and without the Soret effect in the Full-S case. This suggests that the Lewis number effect is mainly responsible for the trend of water vapour reaction rate with strain in the presence of Soret effect.

Consistent with the previous observation, Fig. 10 presents the normalized consumption velocity values (relative to the unstrained flame velocity) for the LNE, PD, and Full cases. Both at $\phi = 0.4$ and $\phi = 0.8$, the normalized consumption velocity values without the Soret effect, as well as the differences between the cases with and without the Soret effect, are qualitatively closer to those of the Full cases. These observations further suggest that the Lewis number effect is primarily responsible for the response of the flame to strain, and the effect of thermal diffusion is to further promote this behaviour. Further insight on how the relative contributions of PD and LNE affect the emissions of NO$_x$ is provided in Section 3.2.3.

3.2. Impact of Soret effect on the NO$_x$ emission prediction

The effect of strain and thermal diffusion modeling on NO$_x$ emissions is investigated in this section. Based on the previous analysis, two representative lean equivalence ratio values have been chosen, namely
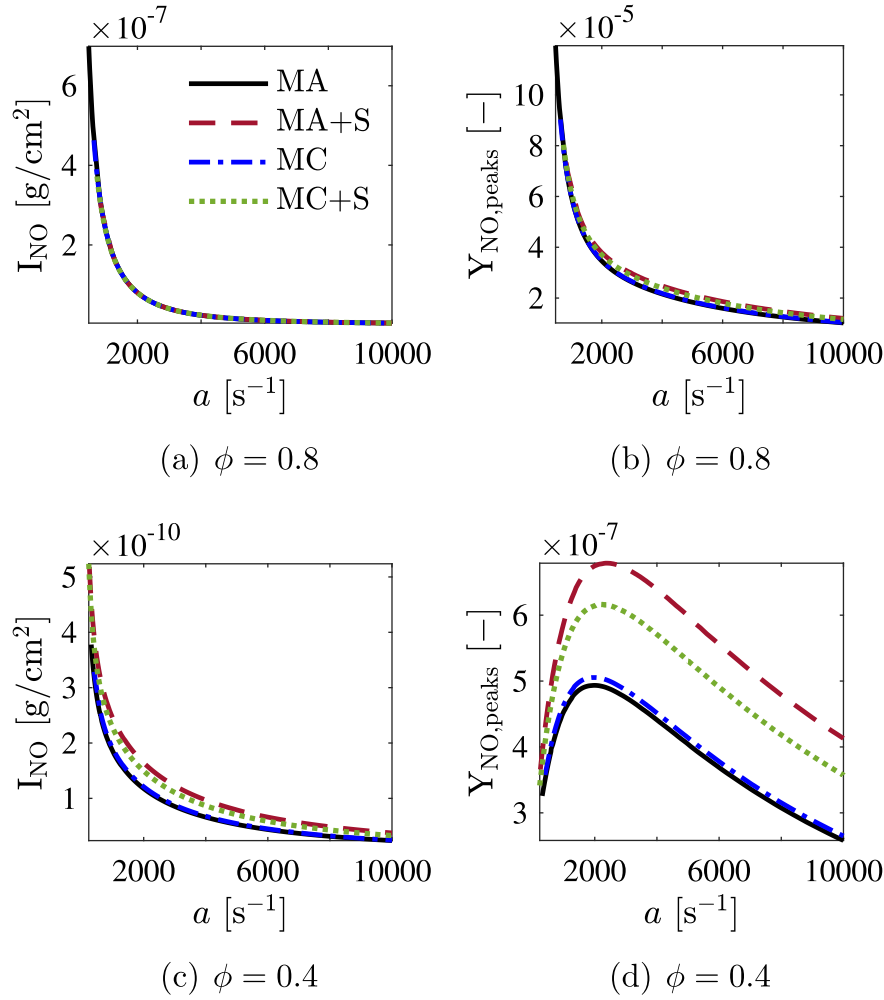
Fig. 12. Density-weighted NO integral I_{NO} and peaks of NO mass fraction Y_{NO} as a function of the applied strain rate a obtained with Mixture Averaged (MA), Mixture Averaged with Soret effect (MA + S), Multi-Component (MC), and Multi-Component with Soret effect (MC + S) diffusion models.

$\phi = 0.8$ and $\phi = 0.4$, in which both the response of the flame to strain and the sensitivity to Soret effect have been found to be different.

3.2.1. NO$_x$ integral and mass fraction distribution

The spatial distribution of the NO mass fraction computed with MA and MA + S models is displayed in Fig. 11. To mitigate uncertainties associated with the choice of the kinetic mechanism for NO$_x$, the trends obtained with the mechanism proposed by Capurso et al. [30] are compared with those obtained using the detailed CRECK mechanism [37]. Although the two kinetic mechanisms differ in the quantitative prediction of the NO profiles, regardless of the diffusion model employed, they consistently predict the same trend with thermal diffusion. Specifically, both at $\phi = 0.8$ (Figs. 11a,b) and $\phi = 0.4$ (Figs. 11c,d), NO profiles show slightly higher peaks when the Soret effect is considered. Additionally, at a fixed equivalence ratio, the NO profiles exhibit greater sensitivity to thermal diffusion at increasing strain rates.

In order to also remove the uncertainties related to the choice of the MA model, the density-weighted NO integral (Fig. 12) and the peaks of NO mass fraction (Fig. 12) are further compared with the MC models with and without the Soret effect. The NO integral is defined as in [13]:

$$I_{NO} = \int_{-L/2}^{L/2} \rho Y_{NO} dx. \tag{10}$$

For all the models considered in the present analysis, it is observed that the integral of NO decreases with increasing strain rate, indicating that lean conditions combined with high strain significantly reduce NO$_x$ emissions. This reduction in NO with strain rate follows the mechanism reported in [13]. Additionally, while all curves collapse for $\phi = 0.8$, suggesting that thermal diffusion has minimal impact on the overall NO level, at $\phi = 0.4$, where the Soret effect strengthens the flame, there is a slight increase in the NO integral. This increase correlates with the higher peaks of NO mass fraction observed at $\phi = 0.4$ compared to the case at $\phi = 0.8$. Thus confirming the relevance of the Soret effect under lean conditions.

3.2.2. Radicals distribution and NO$_x$ overall reaction rate

To gain more insights into the physics behind the overall increase in NO$_x$ emissions with the Soret effect under highly strained conditions, an analysis is conducted on the distribution of the main radicals involved in the NO production pathways. Fig. 13 shows the distribution of the H and O radicals obtained at $\phi = 0.8$ (Figs. 13a,c) and $\phi = 0.4$ (Figs. 13b,d) by varying the applied strain rate from $a = 500$ s^{-1} to $a = 10000$ s^{-1}. Overall, it can be seen that both at $\phi = 0.8$ and $\phi = 0.4$ and at any strain rate investigated, the thermal diffusion leads to higher prediction of O and H radical mass fraction. However, it is evident that this increase is more significant at ultra-lean conditions (Figs. 13b,d). In fact, at $\phi = 0.8$,
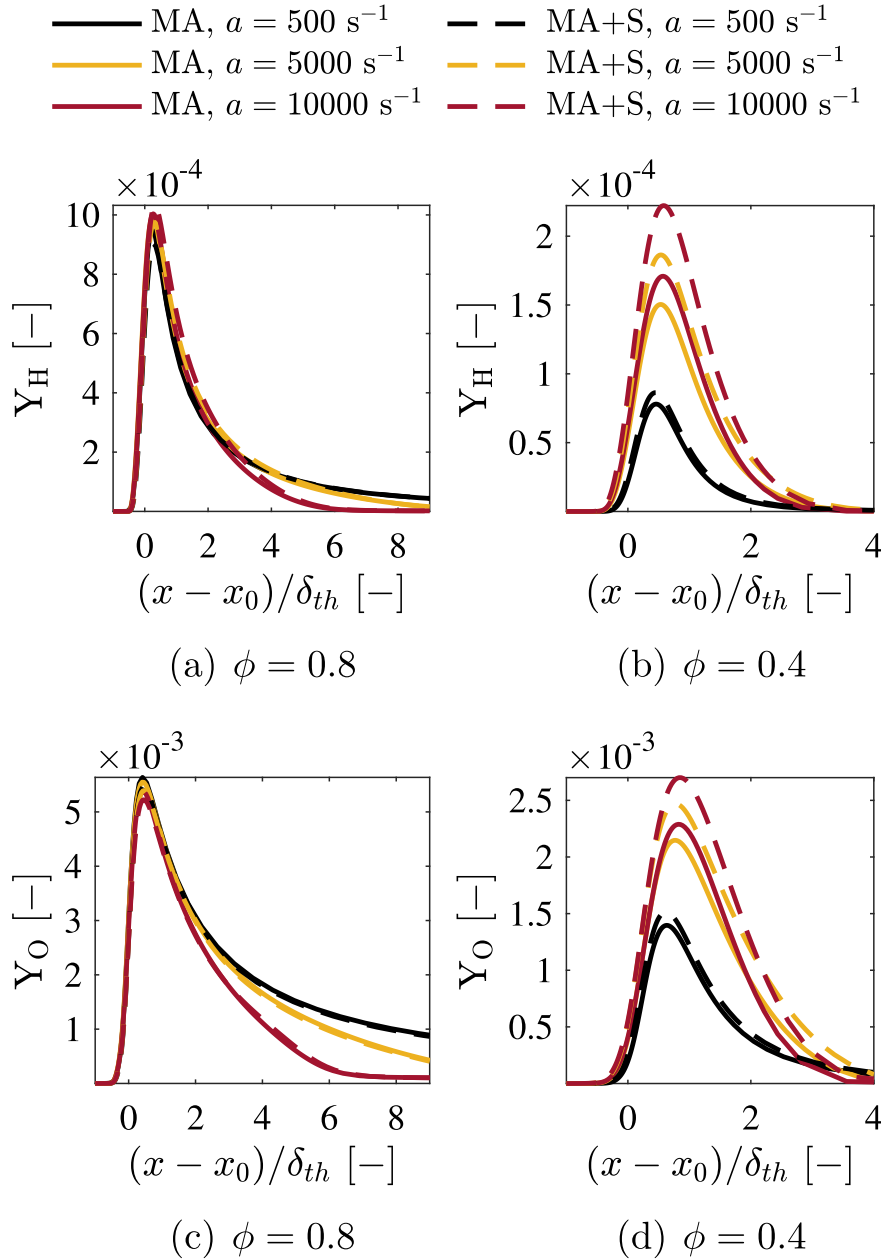
Fig. 13. Distribution of H and O radicals' mass fraction at $\phi = 0.4$ (a),(c) and $\phi = 0.8$ (b),(d) for different applied strain rates a. The acronyms in the legend refer to the Mixture Averaged (MA) and Mixture Averaged with Soret effect (MA + S) diffusion models.

the differences in the peak mass fractions of H and O between the two models are less than 10 % and 2 %, respectively. In contrast, at $\phi = 0.4$, the peak of H radical concentration increases by a factor of 1.3 with MA + S model for the highest strain rate considered, while the O radical peak increases by a factor of 1.1. While the increase of peaks of H radical is due to the net diffusion flux of H that results in its accumulation near the reaction zone (see Figs. 3c,d), the increase of O radical mass fraction can be attributed to the overall increased reactivity of the flame with thermal diffusion.

The role of thermal diffusion in the prediction of NO emission is eventually discussed by analyzing its effect on the NO formation pathways. Data from one-dimensional simulations are used for this purpose, and the NO_x production pathways considered are thermal-NO, the N_2O-NO intermediate, and the NNH-NO. For each route j, the overall reaction rate $ORR_{j,r}$ is computed as in [38]:

$$ORR_{j,r} = \int_{-L/2}^{L/2} \dot\omega_j(x)dx, \qquad (11)$$

where $\dot\omega_{j,r}$ is the net reaction rate of each reaction r across the pathway j. Adding up the contributions along the same route j, the ORR_j is then computed at $\phi = 0.8$ and $\phi = 0.4$ and displayed across the three different pathways in Figs. 14, 15 and 16. Either with or without Soret effect, the thermal NO pathway is observed to remain the dominant mechanism at $\phi = 0.8$ (see Fig. 14a) as the adiabatic flame temperature has exceeded the threshold value that allows the decomposition of N_2 into N radicals. At this equivalence ratio, the effect of strain is to substantially decrease the overall reaction of this pathway due to a re-distribution of the radicals downstream of the flame front [13], where most of the thermal NO_x is formed (see Fig. 11a). When the Soret effect is included, except
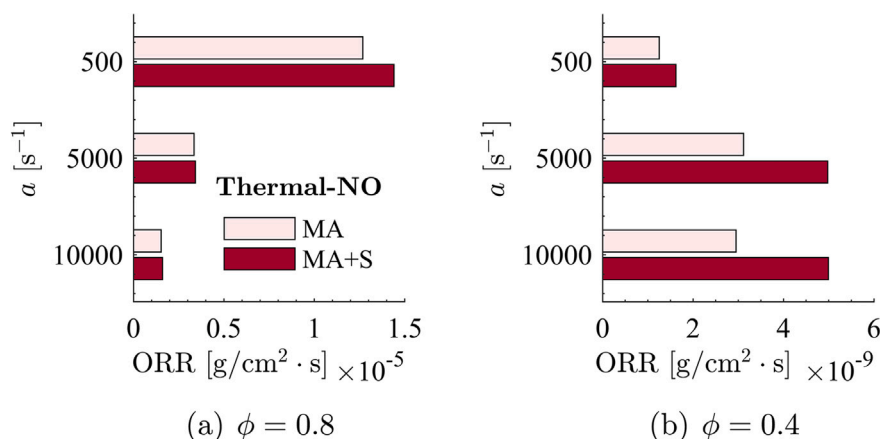
Fig. 14. Overall reaction rate ORR of NO through the thermal pathway at $\phi = 0.8$ (a), and $\phi = 0.4$ (b) for different applied strain rate a values. The acronyms in the legend refer to the Mixture Averaged (MA) and Mixture Averaged with Soret effect (MA + S) diffusion models.

Fig. 15. Overall reaction rate ORR of NO through the N_2O pathway at $\phi = 0.8$ (a), and $\phi = 0.4$ (b) for different applied strain rate a values. The acronyms in the legend refer to the Mixture Averaged (MA) and Mixture Averaged with Soret effect (MA + S) diffusion models.
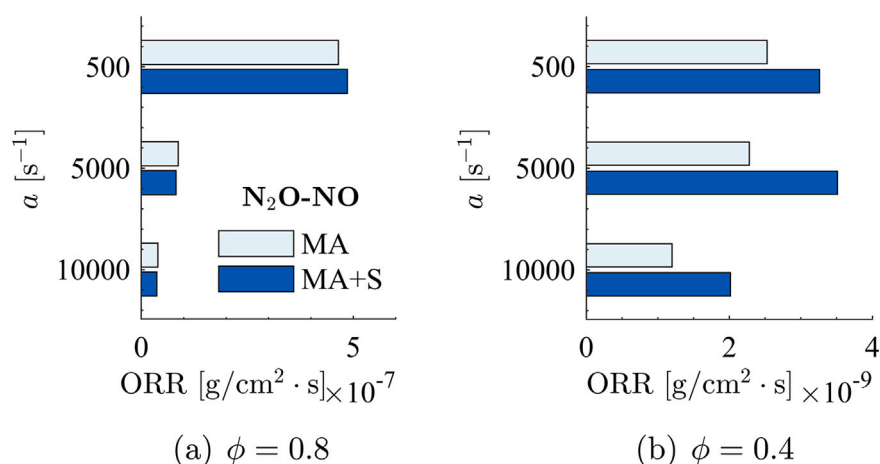
for the NNH route where the NO production rate slightly decreases with thermal diffusion at $\phi = 0.8$ (Fig. 16a), higher ORR values are observed across the N_2O and the dominant thermal pathways. The increase of NO production rate across the thermal route can be attributed either to the behaviour of O radicals controlling the NO formation from such pathway [39] or the temperature. Since the former has been previously observed to have a weak sensitivity to Soret effect at such equivalence ratio (see Fig. 13c), the slight increase of flame temperature with the thermal diffusion (see Fig. 7) is the only responsible for the 10 % increase of the ORR as compared to the case without Soret effect (MA model). On the other hand, at $\phi = 0.4$, which is characterized by a lower adiabatic flame temperature, the NNH pathway becomes dominant, its ORR is observed to increase with strain, and such an increase is further enhanced when thermal diffusion is considered, where the prediction of ORR is up to 30 % higher for the highest strain rate considered. Such a behaviour can be related to the trend of the H radicals with strain when thermal diffusion is accounted for (see Fig. 13b). As already observed, in the presence of thermal diffusion more H radicals are transported into the high-temperature region leading to an increase of the H radicals peaks on the flame (Fig. 13b). Given that within the NNH pathways, H radicals control the formation of NNH from the molecular nitrogen and their diffusion is strongly controlled by Soret effect, this leads to a higher ORR and thus to higher NO peaks (Figs. 11c,d). Furthermore it is interesting to note that, although not the dominant pathways, both the thermal-NO

and N_2O-NO are also influenced by the Soret effect at $\phi = 0.4$. In the case of the thermal pathway, the increase in NO production can be linked to the combined effects of the higher temperatures and peaks in O radical concentration observed with Soret effect at high strain rates. Similarly, as reported in [30], the increased NO production via the N_2O pathway can be also attributed to the higher O radical concentration due to the thermal diffusion, which promotes the low-activation-energy reactions responsible for N_2O formation. In light of the previous analysis, it can be concluded that the lower the equivalence ratio, the stronger the effect of thermal diffusion on the NO_x emissions.

3.2.3. Relative contributions of non-unity Lewis number and preferential diffusion effect on NO_x emissions

In Section 3.1.3, it was observed that the response of the flame to strain is mainly driven by the faster transport of hydrogen, which is further enhanced by Soret diffusion at high strain rates, and that the Lewis number effect is the main driver of this behaviour. A further analysis is performed in this section to shed light on the relative importance between preferential diffusion (PD) and Lewis number effect (LNE) on NO_x emissions. The spatial profiles of the NO mass fraction Y_{NO} obtained by comparing the isolated diffusion mechanisms with and without Soret effect are shown in Fig. 17. Looking at the profiles in the figure, it can be seen that the PD-S curves are closer to the Full-S case either at $\phi = 0.8$ or at $\phi = 0.4$, for any value of applied strain rate studied. In addition,
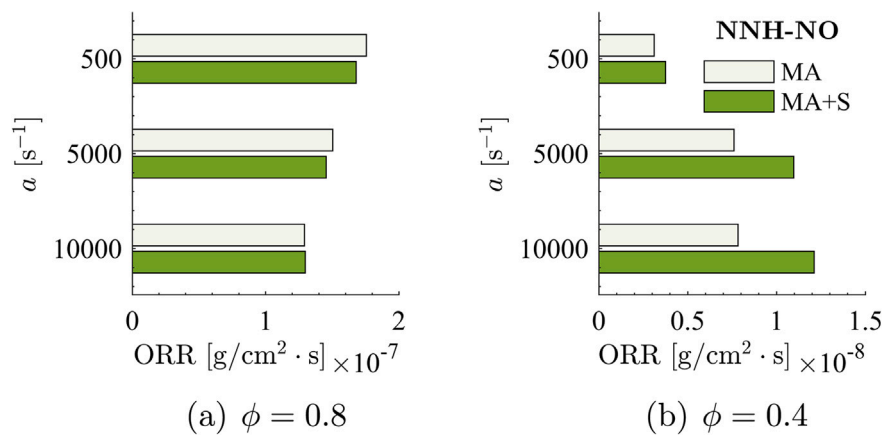
Fig. 16. Overall reaction rate ORR of NO through the NNH pathway at $\phi = 0.8$ (a), and $\phi = 0.4$ (b) for different applied strain rate a values. The acronyms in the legend refer to the Mixture Averaged (MA) and Mixture Averaged with Soret effect (MA + S) diffusion models.
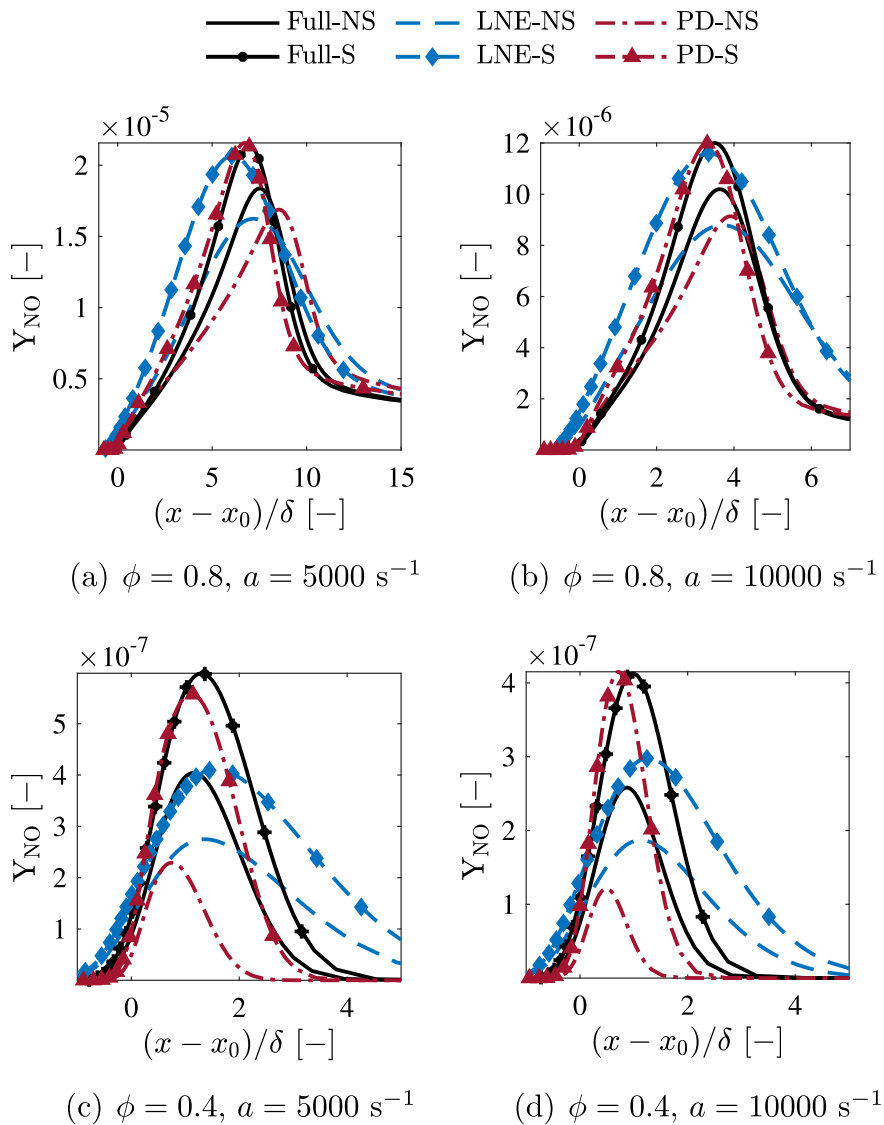

Fig. 17. Spatial profiles of NO mass fraction, Y_{NO}, obtained with and without Soret effect, and by considering both preferential diffusion and Lewis number effects (Full-S and Full-NS cases), or their relative contributions in isolation (PD and LNE cases). The acronyms S and NS refer to inclusion or exclusion of Soret effect respectively.

Fig. 18. NO net production $\dot{\omega}_{NO}$ from the thermal pathway at $\phi = 0.8$ (a) and NNH pathway at $\phi = 0.4$ (b), obtained with and without Soret effect, and by considering both preferential diffusion and Lewis number effects (Full-S and Full-NS cases), or their relative contributions in isolation (PD and LNE cases). The acronyms S and NS refer to inclusion or exclusion of Soret effect respectively. The value of strain rate reported is $a = 10000 \text{ s}^{-1}$.
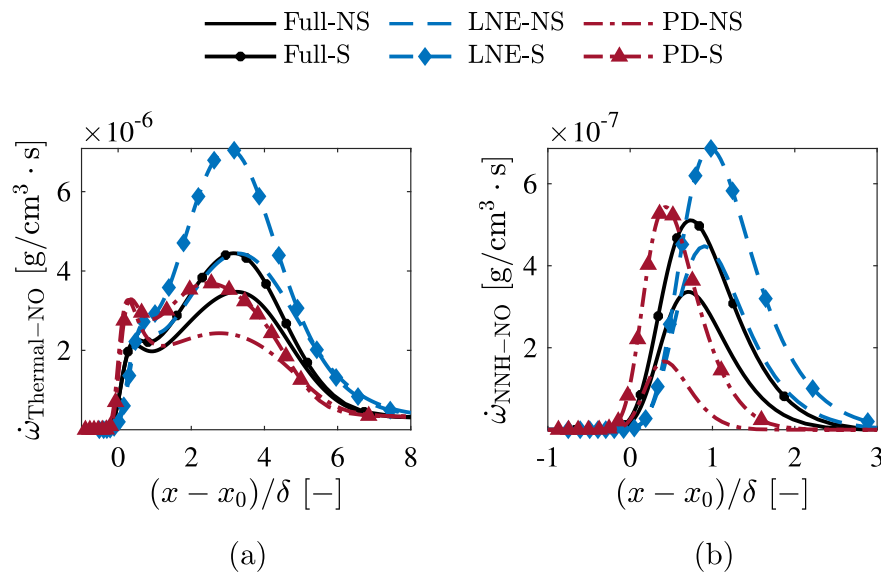
the differences in the peak values of the NO mass fraction with and without Soret effect observed in the Full-NS and Full-S cases seem to be qualitatively closer to those between the PD and PD-S cases. By comparing the results obtained at $\phi = 0.4$ for the two values of strain rate considered (Figs. 17c,d), it can be further seen that, as for the Full-S case, as strain rate increases the PD-S case predicts higher peak values of NO production with respect to the PD-NS case, while a negligible difference is observed between the LNE-NS and LNE-S cases. All these observations suggest that preferential diffusion is the main mechanism responsible for the observed increase of NO with Soret effect at higher strain rates. Further evidence of this is provided in Fig. 18, which displays the local net NO production rate for the dominant NO production pathways at $\phi = 0.8$ (Fig. 18a) and $\phi = 0.4$ (Fig. 18b). Regardless of the equivalence ratio, and thus the dominant NO production pathway, the net local NO production rate predicted by considering only preferential diffusion alongside thermal diffusion aligns more closely with the curve obtained in the Full-S case. In contrast, modeling only the Lewis number effect with Soret effect would significantly overestimate the global NO production. Thus, unlike the flame's response to strain, which is primarily governed by the non-unity Lewis number effect, preferential diffusion plays a more significant role in the evolution of NO_x emissions with strain, and the Soret effect further amplifies this influence. In fact, thermal diffusion is also observed to significantly enhance the local variation in the equivalence ratio, which is primarily an effect of preferential diffusion. This variation in local stoichiometry leads to a locally-reacher flame, which in turn results into a higher concentration of the H (Fig. 13b), O (Fig. 13d), and OH (not shown) radicals. At ultra-lean conditions, the higher H radicals concentration, further focused near the reaction zone by their thermal diffusion, contributes to the increased NO production through the NNH pathway (see Fig. 16b). Similarly, at moderately lean conditions, where NO is predominantly formed through the thermal pathway (see Fig. 14a), the Soret effect increases the NO formation rate due to the elevated temperature resulting from the local variation of the equivalence ratio.

3.2.4. Effect of pressure

The flame's response to strain can be enhanced at high pressure (see for example Fig. 6 in [40]). One may then argue that higher pressure conditions also amplify the flame sensitivity to the Soret effect. The influence on NO_x emissions is however more complex to extrapolate, as the

NO production pathways change according to the pressure as well. For this reason, some light is shed in this section on the impact of thermal diffusion on flame structure and NO_x emissions as pressure increases. To illustrate this, Fig. 19 displays the overall reaction rate ORR of NO obtained across the thermal, N_2O and NNH pathways at a pressure of 10 bar and equivalence ratios $\phi = 0.8$ (Fig. 19 left column) and $\phi = 0.4$ (Fig. 19 right column). It is important to note that the chemical mechanism employed for this analysis is verified to accurately predict the overall NO profile at high-pressure conditions (see Fig. A1c in the supplementary material of [30]). At 10 bar, NO production increases across all the pathways considered, and the thermal pathway remains the dominant route of NO production at $\phi = 0.8$. As also observed for atmospheric conditions (Fig. 14a), at 10 bar the thermal diffusion increases the net global production of NO as compared to the case where thermal diffusion is not accounted for. Specifically, the highest deviation between the MA and MA+S models at high pressure is about 58 % at $a = 500 \text{ s}^{-1}$, which can be attributed to the increased maximum temperature when thermal diffusion is considered. At $\phi = 0.4$, the N_2O pathway becomes a dominant contributor to the NO production at 10 bar, and the Soret effect remains significant in enhancing this production, leading to a deviation up to 37 % between the MA and MA+S cases. As discussed in Section 3.2.2, this deviation can be attributed to the elevated peaks of the O radical under the influence of the Soret effect at high pressure (not shown), which promote low-activation-energy reactions responsible for N_2O formation.

4. Conclusion

The influence of thermal diffusion on flame behaviour and NO_x emissions in lean strained hydrogen/air premixed flames has been investigated in a reactant-to-product counterflow flame configuration by employing detailed-chemistry one-dimensional simulations. The results showed that the sensitivity of strained flames to Soret effect depends on the range of equivalence ratios considered. As the mixture becomes leaner, the flame becomes more sensitive to strain, and the addition of Soret effect further enhances the flame sensitivity to strain due to its coupling with preferential diffusion. Consistently, the thermal diffusion is shown to increase the peaks of temperature, which makes the flame even more resistant to very high strain rates. Furthermore, it has been found that at moderately lean conditions, even though the flame response is
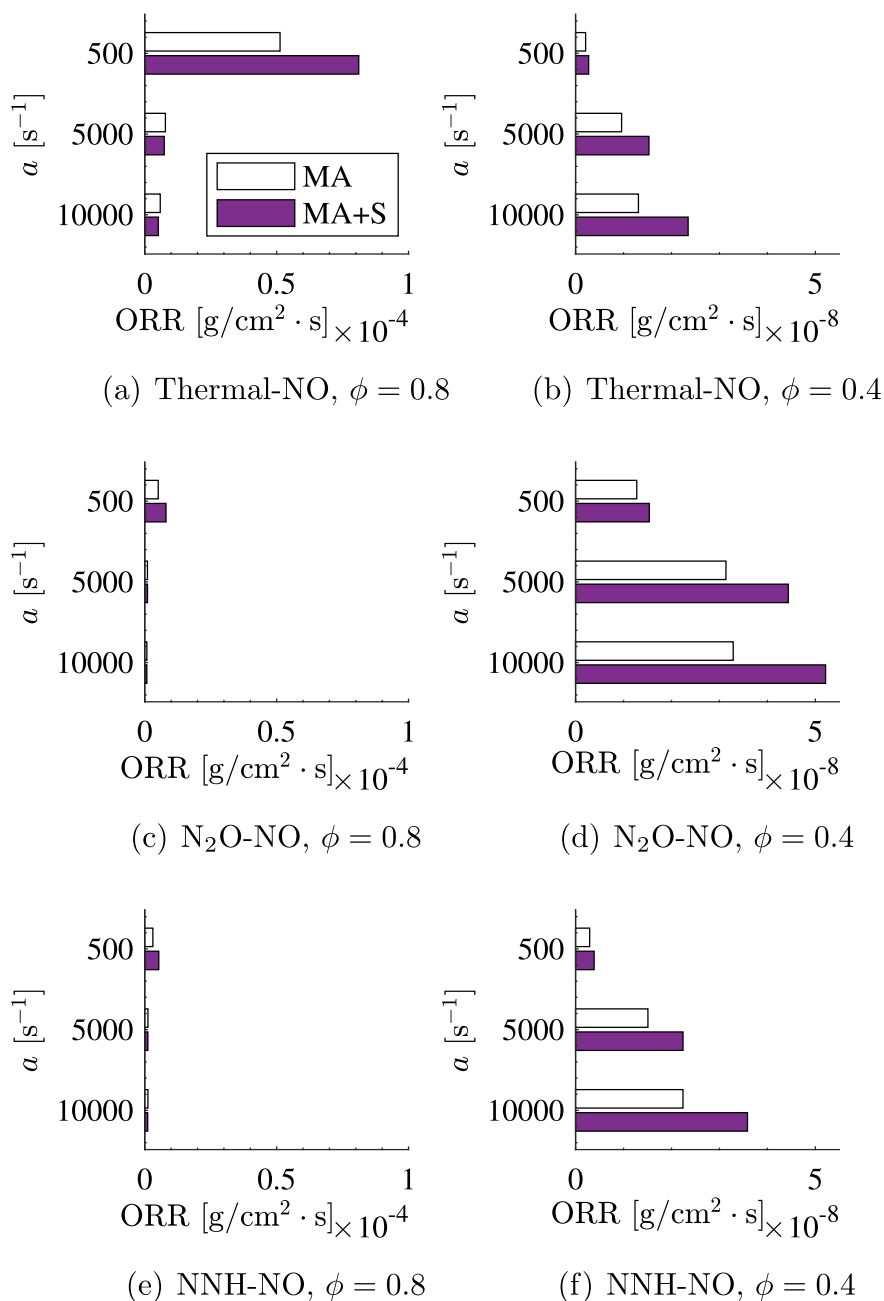
Fig. 19. Overall reaction rate ORR across the thermal, N₂O, and NNH pathways at pressure $p = 10$ bar. The acronyms in the legend refer to the Mixture Averaged (MA) and Mixture Averaged with Soret effect (MA + S) diffusion models.

less sensitive to strain, the Soret effect still plays a role, contributing to the transport of the light species towards the high-temperature region. Moreover, the thermal diffusion is observed to shift the peak of consumption speed towards higher strain rate values, thus shifting the inversion point of the Markstein length towards higher values of equivalence ratio. These behaviours are shown to be mostly linked to the Soret effect enhancing the Lewis number effect.

As thermal diffusion can alter the behaviour of strained flames, particularly under ultra-lean conditions, the prediction of NO_x emissions is also affected. The inclusion of thermal diffusion in the modeling is found to affect the peak value of NO mass fraction and its formation rate independently of the chemical mechanism employed. At atmospheric conditions, the inclusion of thermal diffusion in the modeling has revealed that the peaks of NO mass fraction experience an increase, which

is more pronounced in ultra-lean conditions where Soret effect strengthens the flame. The trend of NO production rate with strain is also affected. The prediction mismatch ranges from 10 % across the thermal pathway in moderately lean conditions up to 30 % in ultra-lean conditions where the NNH pathway is dominant. In fact, the prediction of NO formed across the NNH route is strongly affected by the accuracy of the local radicals concentration. Moreover, it has been found that, at the lean and ultra-lean conditions examined, the trends of NO_x production rate with strain rate are mainly linked to hydrogen's preferential diffusion. Eventually, results obtained for high-pressure conditions confirm the importance of modeling thermal diffusion under highly strained conditions even at elevated pressure as the discrepancies in the computation of the global production rate range from 37 % for ultra-lean up to 50 % for moderate lean conditions.

CRediT authorship contribution statement

Maria Rosaria Acquaviva: Writing – review & editing, writing – original draft, investigation, formal analysis, and conceptualization. **Alessandro Porcarelli:** Writing – review & editing, supervision, methodology, and conceptualization. **Ivan Langella:** Writing – review & editing, supervision, and funding acquisition.

Declaration of Competing Interest

The authors declare that they have no known competing financial interests or personal relationships that could have appeared to influence the work reported in this paper.

Acknowledgments

Data availability

Data will be made available on request.

References

[1] Singla MK, Nijhawan P, Oberoi AS. Hydrogen fuel and fuel cell technology for cleaner future: a review. Environ Sci Pollut Res 2021;28(13):15607–26.

[2] EU Green Deal. The European green deal. Technical report. European commission; 2020.

[3] Barbosa FC. Zero carbon emission aviation fuel technology review-the hydrogen pathway. Technical report. FCB Research; 2024.

[4] Lipatnikov AN, Chomiak J. Molecular transport effects on turbulent flame propagation and structure. Prog Energy Combust Sci 2005;31(1):1–73.

[5] Pitsch H. The transition to sustainable combustion: hydrogen-and carbon-based future fuels and methods for dealing with their challenges. Proc Combust Inst 2024;40(1):105638.

[6] Matalon M. Intrinsic flame instabilities in premixed and nonpremixed combustion. Annu Rev Fluid Mech 2007;39(1):163–91.

[7] Regele JD, Knudsen E, Pitsch H, Blanquart G. A two-equation model for non-unity Lewis number differential diffusion in lean premixed laminar flames. Combust Flame 2013;160(2):240–50.

[8] Lee HC, Dai P, Wan M, Lipatnikov AN. Lewis number and preferential diffusion effects in lean hydrogen–air highly turbulent flames. Phys Fluids 2022 03; 34(3):035131.

[9] Porcarelli A, Langella I. Mitigation of preferential diffusion effects by intensive strain in lean premixed hydrogen flamelets. Proc Combust Inst 2024;40(1):105728.

[10] Rahman MA, Saghir MZ. Thermodiffusion or soret effect: historical review. Int J Heat Mass Transfer 2014;73:693–705.

[11] Ern A, Giovangigli V. Impact of detailed multicomponent transport on planar and counterflow hydrogen/air and methane/air flames. Combust Sci Technol 1999;149(1–6):157–81.

[12] Zhou Z, Hernández-Pérez FE, Shoshin Y, van Oijen Ja, de Goey Lph. Effect of Soret diffusion on lean hydrogen/air flames at normal and elevated pressure and temperature. Combust Theory Model 2017;21(5):879–96.

[13] Porcarelli A, Kruljević B, Langella I. Suppression of NO_x emissions by intensive strain in lean premixed hydrogen flamelets. Int J Hydrog Energy 2024;49:413–31.

[14] Williams BA. Sensitivity of calculated extinction strain rate to molecular transport formulation in nonpremixed counterflow flames. Combust Flame 2001;124(1–2):330–333.

[15] Liang W, Chen Z, Yang F, Zhang H. Effects of Soret diffusion on the laminar flame speed and Markstein length of syngas/air mixtures. Proc Combust Inst 2013;34(1):695–702.

[16] Garcia-Ybarra P, Nicoli C, Clavin P. Soret and dilution effects on premixed flames. Combust Sci Technol 1984;42:87–109.

[17] Yang F, Law CK, Sung CJ, Zhang HQ. A mechanistic study of soret diffusion in hydrogen–air flames. Combust Flame 2010;157(1):192–200.

[18] Acampora L, Marra FS. Effects of soret diffusion on the exergy losses in hydrogen laminar premixed flames. Int J Hydrog Energy 2023;48(73):28539–48.

[19] Grcar JF, Bell JB, Day MS. The Soret effect in naturally propagating, premixed, lean, hydrogen–air flames. Proc Combust Inst 2009;32(1):1173–80.

[20] D'Alessio F, Matteucci C, Lapenna PE, Creta F. Intrinsic instability of lean hydrogen/ammonia premixed flames: influence of soret effect and pressure. Fuel Commun 2024;19:100110.

[21] D'Alessio F, Lapenna PE, Bottari S, Creta F. Intrinsically unstable hydrogen-enriched premixed ammonia flames: analysis and modeling of NO formation. Proc Combust Inst 2024;40(1):105485.

[22] Wen A, Berger L, Vom Lehn F, Parente A, Pitsch H. Numerical analysis and flamelet modeling of NO_x formation in a thermodiffusively unstable hydrogen flame. Combust Flame 2023;253:112817.

[23] Marzouk YM, Speth RL, Ghoniem AF. Combined effects of curvature and strain on hydrogen enriched lean methane flames. Technical report, Sandia National Lab.(SNL-CA). Livermore, CA (United States): 2005.

[24] Eindhoven University of Technology. CHEM1D a one dimensional laminar flame code; 2021. https://github.com/thijsa93400/TUe_chem1d

[25] van Oijen Ja, Donini A, Bastiaans RJM, ten Thije Boonkkamp Jhm, de Goey Lph. State-of-the-art in premixed combustion modeling using flamelet generated manifolds. Prog Energy Combust Sci 2016;57:30–74.

[26] Curtiss CF, Hirschfelder JO. Transport properties of multicomponent Gas mixtures. J Chem Phys 1949 06; 17(6):550–55.

[27] Evlampiev A. *Numerical combustion modeling for complex reaction systems*. Phd thesis 1 (Research TU/e / graduation TU/e). Mech Eng 2007.

[28] Schlup J, Blanquart G. A reduced thermal diffusion model for H and H_2. Combust Flame 2018;191:1–8.

[29] Mechanical and Aerospace Engineering (Combustion Research) University of California at San Diego. Chemical-kinetic mechanisms for combustion applications; 2003. http://maeweb.ucsd.edu/combustion/cermech/.

[30] Capurso T, Laera D, Riber E, Cuenot B. NO_x pathways in lean partially premixed swirling H_2-air turbulent flame. Combust Flame 2023;248:112581.

[31] Chen YC, Bilger RW. Experimental investigation of three-dimensional flame-front structure in premixed turbulent combustion—I: hydrocarbon/air bunsen flames. Combust Flame 2002;131(4):400–35.

[32] Ern A, Giovangigli V. Thermal diffusion effects in hydrogen-air and methane-air flames. Combust. Theory Modelling 1998;2(4):349.

[33] Law CK. Dynamics of stretched flames. Symp (Int) Combust 1989;22(1):1381–402.

[34] Bradley D, Gaskell PH, Gu XJ. Burning velocities, Markstein lengths, and flame quenching for spherical methane-air flames: a computational study. Combust Flame 1996;104(1):176–98.

[35] Böttler H, Kaddar D, Karpowski TJP, Ferraro F, Scholtissek A, Nicolai H, et al. Can flamelet manifolds capture the interactions of thermo-diffusive instabilities and turbulence in lean hydrogen flames?—an a-priori analysis. Int J Hydrogen Energy 2024;56:1397–407.

[36] Lee HC, Dai P, Wan M, Lipatnikov AN. Lewis number and preferential diffusion effects in lean hydrogen–air highly turbulent flames. Phys Fluids 2022 03; 34(3):035131.

[37] Ranzi E, Frassoldati A, Stagni A, Pelucchi M, Cuoci A, Faravelli T. Reduced kinetic schemes of complex reaction systems: fossil and biomass-derived transportation fuels. Int J Chem Kinet 2014;46(9):512–42.

[38] Ning D, Fan A, Yao H. Effects of fuel composition and strain rate on NO emission of premixed counterflow H_2/CO/air flames. Int J Hydrog Energy 2017;42(15):10466–74.

[39] Zeldovich YA, Frank-Kamenetskii D, Sadovnikov P. Oxidation of nitrogen in combustion. Publishing House of the Acad of Sciences of USSR; 1947.

[40] Rieth M, Gruber A, Chen JH. The effect of pressure on lean premixed hydrogen-air flames. Combust Flame 2023;250:112514.